



Published in final edited form as:

Top Magn Reson Imaging. 2016 October ; 25(5): 187–196. doi:10.1097/RMR.000000000000104.

MR molecular imaging of brain cancer metabolism using hyperpolarized ^{13}C magnetic resonance spectroscopy

Chloé Najac¹ and Sabrina M. Ronen^{1,✉}

¹Department of Radiology and Biomedical Imaging, University of California San Francisco, San Francisco, CA, USA

Abstract

Metabolic reprogramming is an important hallmark of cancer. Alterations in many metabolic pathways support the requirement for cellular building blocks that are essential for cancer cell proliferation. This metabolic reprogramming can be imaged using magnetic resonance spectroscopy (MRS). ^1H MRS can inform on alterations in the steady-state levels of cellular metabolites, but the emergence of hyperpolarized ^{13}C MRS has now also enabled imaging of metabolic fluxes in real-time, providing a new method for tumor detection and monitoring of therapeutic response. In the case of glioma, preclinical cell and animal studies have shown that the hyperpolarized ^{13}C MRS metabolic imaging signature is specific to tumor type and can distinguish between mutant IDH1 glioma and primary glioblastoma. Here, we review these findings, first describing the main metabolic pathways that are altered in the different glioma subtypes, and then reporting on the use of hyperpolarized ^{13}C MRS and MR spectroscopic imaging (MRSI) to probe these pathways. We show that the future translation of this hyperpolarized ^{13}C MRS molecular metabolic imaging method to the clinic promises to improve the noninvasive detection, characterization, and response-monitoring of brain tumors resulting in improved patient diagnosis and clinical management.

Keywords

glioma; metabolic reprogramming; hyperpolarized ^{13}C ; magnetic resonance spectroscopy

Introduction

Gliomas are the most common type of brain tumor, representing 80% of all diagnosed malignant central nervous system tumors in the United-States ¹. They are classified into three categories – astrocytoma, oligodendroglioma and glioblastoma – and four World Health Organization grades – I to IV – based on clinical and pathological criteria ^{1,2}. Grade I tumors are typically benign. Grade II tumors are referred to as low-grade in contrast to grades III and IV tumors that are considered higher-grade. Glioblastoma (GBM) is a grade IV glioma that accounts for more than 50% of all diagnosed gliomas ¹. It is the most aggressive type of glioma and is associated with a very poor prognosis with a median

✉Corresponding author: Sabrina M. Ronen, 1700 4th Street, Byers Hall 303E, University of California San Francisco, San Francisco, CA 94143. sabrina.ronen@ucsf.edu.

survival time of 15 months¹. 90% of all GBM develop rapidly *de novo* and are referred to as primary GBM. The rest progress from grade II or III astrocytoma and are referred to as secondary or upgraded GBM^{3,4}. Oligodendroglioma tumors present only as grade II or III and do not evolve to secondary GBM. Grades II and III astrocytoma and oligodendroglioma have a relatively better prognosis than GBM². Current standard of care for brain tumors is a combination of treatments that depends on tumor type and grade and includes surgical resection, radiation therapy and chemotherapy, with immunotherapy and targeted therapies presenting new therapeutic approaches.

Independent of their histology or prognosis, oligodendroglioma, astrocytoma and secondary GBM differ significantly in their genetic and epigenetic signatures from primary GBM. Primary GBM are driven by multiple genetic alterations such as loss of the phosphatase and tensin homolog (PTEN) gene, amplification or mutation of the epidermal growth factor receptor (EGFR), and increased signaling via the phosphatidylinositol-3-kinase (PI3K)/Akt pathway^{2,5}. In contrast, 70–90% of grade II/III glioma and secondary GBM harbor a mutation in the cytosolic isocitrate dehydrogenase 1 gene (IDH1)^{6–9}. This recently discovered mutation, identified as a single amino acid substitution at arginine 132^{6–9}, is one of the earliest genetic events in low-grade tumors, and has been shown to drive tumor development. All mutations are heterozygous leading to the retention of the wild-type form of the isocitrate dehydrogenase enzyme, responsible for the conversion of isocitrate to alpha-ketoglutarate (α -KG). However, mutant IDH1 inhibits the wild-type form and establishes a new function converting α -KG to 2-hydroxyglutarate (2-HG). Production of elevated levels of 2-HG leads to epigenetic alterations which, in turn, lead to the development of oligodendroglioma and astrocytoma tumors¹⁰. In addition to the IDH1 mutation, over 70% of grade II/III astrocytomas and oligodendrogliomas have a mutation in the TP53 tumor suppressor gene and a co-deletion of chromosome arms 1p/19q respectively^{2,11}.

Magnetic resonance imaging (MRI) is the main imaging modality used to diagnose and grade brain tumors. In the clinic, T1-weighted imaging pre- and post-injection of gadolinium, T2-weighted imaging, fluid-attenuated inversion recovery imaging, diffusion-weighted imaging and dynamic susceptibility-weighted contrast-enhanced imaging are the most commonly used MRI methods^{12–14}. However, although they provide crucial information on the structure and perfusion of the tumor as well as the integrity of the blood-brain barrier (BBB), these methods do not provide metabolic information on the lesions. ¹H magnetic resonance spectroscopy (MRS) *in vivo* or in biopsy samples allows probing steady-state metabolite levels, and several studies have demonstrated the potential of ¹H MRS to differentiate tumors from normal brain and non-neoplastic lesions^{13,15–19}. Tumors are usually associated with high levels of choline-containing metabolites (comprised of choline, phosphocholine (PC) and glycerophosphocholine (GPC)) and low levels of N-acetyl-aspartate as well as an increase in lactate level in high-grade tumors^{13,17}. Recently, using ¹H MRS, the oncometabolite 2-HG produced by mutant IDH1 was detected *in vivo* in glioma patients harboring the IDH1 mutation^{20–23} as well as *ex vivo* in glioma biopsies^{24,25}. ¹³C MRS can provide additional information in the study of brain tumor metabolism by monitoring metabolic fluxes²⁶. However, ¹³C MRS studies have been more challenging due to the significantly lower intrinsic sensitivity of the technique. The natural abundance of ¹³C is only 1.1% and its gyromagnetic ratio, $\gamma_{13C}=10.705$ MHz/T, is ~ 4 times

lower than γ_{1H} . As a result, even when using ^{13}C -labeled compounds long acquisition times are required limiting the application of this method for patient studies. The emergence of hyperpolarized ^{13}C MRS has opened a range of new possibilities for novel metabolic imaging studies that are translatable to the clinic and can serve to characterize brain tumors and their response to therapy^{27–30}.

Here, we will first describe the main metabolic pathways that are altered in brain cancers. We will focus primarily on the pathways that have been investigated using hyperpolarized ^{13}C MRS. Then, we will briefly describe the principles of hyperpolarized ^{13}C MRS and discuss the main agents developed to monitor the metabolism of brain tumor cells. Tables 1 and 2 and Figure 1 summarize the ^{13}C -labeled probes that have been hyperpolarized using the DNP technique and applied to the study of metabolic reprogramming in cell models and *in vivo* preclinical models of brain tumors.

Metabolic reprogramming in brain tumors

Cancer cells have the ability to adapt their metabolism to enhance survival. Most notably, they alter their glucose metabolism, up-regulating glucose uptake to produce elevated lactate levels even under aerobic condition^{31,32}. This phenomenon is known as the “Warburg effect”, and was first described by Otto Warburg in 1926³¹. Elevated glucose uptake and glycolytic activity serve to acidify the environment, promoting metastasis³³, and to generate the building-blocks necessary to support rapid cell proliferation and tumor survival, such as nucleotides, amino acids and lipids^{34,35}. Importantly, and contrary to Warburg’s initial hypothesis, the glycolytic switch does not result from defective mitochondria but from metabolic reprogramming that has recently been recognized as one of the ten hallmarks of cancer³⁶. This metabolic reprogramming depends upon the activation of several oncogenic signaling pathways, proto-oncogenes and tumor suppressors³². As mentioned above, the activated pathways vary significantly between brain tumor subtypes resulting in metabolic reprogramming that is also unique.

In the case of primary GBM, the PI3K/Akt pathway is activated in more than 88% of cases^{5,37}. The increased activity of this pathway is associated with tumor progression and resistance to cancer therapies³⁸. At the same time, activation of the PI3K/Akt pathway leads to an increase in glucose transporter expression and up-regulation of glycolysis³². It also promotes lipid synthesis facilitating conversion of mitochondrial citrate to acetyl-coA by activating the expression of the enzyme citrate lyase³². Downstream of PI3K/Akt, mammalian target of rapamycin complex 1 (mTORC1) facilitates anabolic processes including protein synthesis and lipid synthesis, and limits autophagy³². mTORC1 also regulates the activity of hypoxia-inducible factor-1 alpha (HIF-1 α), a major player in mitochondrial metabolism³². Stabilization of HIF-1 α in cancer cells drives the expression of pyruvate dehydrogenase kinase 1 (PDK1) that leads to phosphorylation and inhibition of pyruvate dehydrogenase activity (PDH). Inhibition of PDH, in turn, blocks the entry of pyruvate into the tricarboxylic acid (TCA) cycle and therefore limits glucose-dependent TCA metabolism³². Another key role of HIF-1 α in cancer cells is to up-regulate monocarboxylate transporters (MCTs)³⁹. Over-expression of MCTs is crucial to help maintain the hyper-glycolytic and acid-resistant phenotypes⁴⁰. Whereas MCT1 and MCT2

have a high-affinity for the influx of pyruvate, MCT4 is mostly associated with the export of lactate protecting the intracellular environment from acidification while reducing the extracellular pH⁴⁰. Thus, although lactate production can vary significantly amongst brain tumors, GBM typically exhibit elevated lactate levels^{31,41,42}. The PI3K-Akt pathway and HIF-1 α also modulate choline metabolism in GBM. Similar to other cancers⁴³ PC, which is generated by choline phosphorylation via choline kinase and is the precursor of the main membrane phospholipid phosphatidylcholine (PtdCho), is significantly increased in GBM⁴⁴. This reflects the requirement of proliferating cancer cells for membrane synthesis, and the interplay between choline metabolism and oncogenic processes^{43,45}. Finally, a large proportion of GBM over-express the oncogenic transcription factor Myc, which also impacts mitochondrial metabolism^{46,47}. Myc stimulates glutamine uptake and glutamine mitochondrial utilization by increasing the expression of glutaminase, the enzyme that converts glutamine to glutamate^{32,48,49}. Recent studies also reported an increase in acetate uptake and conversion to acetyl-CoA correlating with up-regulation of acetyl-CoA synthase enzyme 2 in GBM^{50–52}.

As mentioned above, primary GBM differ genetically from mutant IDH1-driven low-grade gliomas (astrocytoma and oligodendroglioma) and secondary GBM. As a result, the metabolic reprogramming of these tumors is also different. Similarly to primary GBM, low-grade gliomas have been characterized by an elevated total choline pool. However, more recent studies looking at events specifically associated with the IDH1 mutation, have demonstrated that GPC levels are elevated in these cells and that PC levels are reduced compared to wild-type IDH1 cells^{44,53–55}. The link to mutant IDH1 remains to be determined. Other metabolic alterations detected in mutant IDH1 gliomas have been directly linked to elevated 2-HG levels. It has been shown that accumulation of 2-HG leads to hypermethylation of the branched chain amino acid transferase (BCAT) 1 promoter reducing the activity of the enzyme responsible for the conversion of α -KG to glutamate⁵⁶. The IDH1 mutation also leads to the hypermethylation and consequently silencing of lactate dehydrogenase A (LDHA), the enzyme that converts pyruvate to lactate⁴². Additionally, reduced expression of MCT1 and MCT4 is observed in mutant IDH tumors^{42,57}. We also recently observed a reduction in PDH activity that was associated with increased PDK3 expression downstream of HIF-1 α stabilization by 2-HG⁵⁸. Finally, as a result of the reduced activity of wild-type IDH1, and the increased activity of NADPH-dependent mutant IDH1, levels of NADPH are also diminished in mutant IDH1 glioma cells as are the levels of glutathione (GSH), leading to elevated levels of reactive oxygen species (ROS)⁵⁹.

Hyperpolarized ¹³C MRS: imaging brain tumor status

The emergence of hyperpolarized ¹³C MRS enables monitoring of metabolic pathways and their alterations in a non-invasive and non-ionizing manner. Molecules containing NMR-visible nuclei, such as ¹³C or ¹⁵N, can be hyperpolarized using dissolution dynamic nuclear polarization (DNP). The dissolution DNP method allows hyperpolarization and dissolution of ¹³C-labeled compounds resulting in an increase in their signal-to-noise ratio (SNR) by 10,000 to 50,000-fold as compared to thermal equilibrium^{27,30,60}. To achieve this, the labeled compound, mixed with a free radical, is placed at low temperature (<2K) and at high magnetic field (~3–5T). Microwave irradiation then saturates the electron spin resonance

and polarization is transferred from the radical electron to the labeled nucleus^{27,2}. This leads to an increase in polarization from parts per million to 10–50%. However, a limitation of hyperpolarized agents is their lifetime, or the longitudinal T1 relaxation time of the polarized carbons, which determines how fast the polarization is lost after dissolution. Relaxation times are typically less than a minute. A meaningful brain study therefore requires rapid dissolution and injection of the hyperpolarized agents, as well as rapid transport across the BBB and a fast metabolic rate. In addition, a rapid data acquisition strategy is required with minimal excitation of the injected hyperpolarized labeled compound and optimal excitation of the downstream metabolic products, as each excitation results in an accelerated and non-renewable decay of the hyperpolarization^{30,61–65}. This has led to a trade-off between spatial resolution and acquisition time³⁰. In spite of these challenges, several hyperpolarized ¹³C agents as well as novel imaging methods have been developed over the past decade to specifically image metabolism including the aforementioned metabolic pathways that are reprogrammed in brain tumors (see Figure 1 and Tables 1 and 2).

Pyruvate at the “cross-roads” of several metabolic pathways

[1-¹³C]-pyruvate is the poster-child of hyperpolarized ¹³C probes. It has a relatively long T1 (~67s at 3T), a high polarization level (up to 40%)⁶⁶, and is also highly biologically relevant. Pyruvate is the end product of glucose degradation and at the intersection of several metabolic pathways that are altered in brain tumors. As mentioned previously, GBMs are characterized by their up-regulation of aerobic glycolysis (also known as the “Warburg” effect)³¹ via increased expression of LDHA, the enzyme that converts pyruvate into lactate, and decreased activity of PDH, the enzyme responsible for pyruvate flux into the TCA cycle. In contrast, in low-grade mutant IDH1 tumors, LDHA is silenced⁴². Hyperpolarized [1-¹³C]-pyruvate can be used to monitor LDHA and PDH status by monitoring the production of [1-¹³C]-lactate and [¹³C]-bicarbonate respectively (Figure 1). During the past decade there has also been a growing interest in using hyperpolarized [2-¹³C]-pyruvate to monitor TCA cycle flux by probing for [5-¹³C]-glutamate formation simultaneously with the production of [2-¹³C]-lactate (Figure 1). Similarly to [1-¹³C]-pyruvate, [2-¹³C]-pyruvate fulfills the technical requirements for hyperpolarized studies (T1~40s at 3T and polarization level up to 27%)³⁰. However, its use in the study of brain tumors *in vivo*, as well as other organs, has been limited due to the relatively low SNR of [5-¹³C]-glutamate and the requirement for a wide spectral window compared to studies with [1-¹³C]-pyruvate (~24ppm between [2-¹³C]-pyruvate and [5-¹³C]-glutamate or 136ppm between [2-¹³C]-pyruvate and [2-¹³C]-lactate compared to only ~12 ppm between [1-¹³C]-pyruvate and [1-¹³C]-lactate)³⁰.

[1-¹³C]-pyruvate

Different acquisition strategies have been developed and used to monitor the metabolic conversion of [1-¹³C]-pyruvate as previously reviewed in detail³⁰. Briefly, dynamic data sets from live cells have been obtained by acquiring sequential spectra using a pulse-acquire sequence with a low flip angle^{57,67–69}. *In vivo* animal brain tumor studies have been performed using either dynamic or single time point 2D chemical shift imaging (CSI) with low flip angle^{70,71}. An alternate approach used is single time point 2D MR spectroscopic

imaging using a double spin echo RF pulse with variable flip angles^{72,73} (see Tables 1 and 2).

Elevated hyperpolarized [1-¹³C]-lactate production following the injection of hyperpolarized [1-¹³C]-pyruvate was detected in several preclinical orthotopic GBM models compared to normal brain^{67,70,72-74}. In contrast, in a low-grade IDH1 mutant orthotopic tumor model where LDHA is silenced⁴², very low production of hyperpolarized [1-¹³C]-lactate was observed⁶⁹. Other studies showed a decreased level of hyperpolarized [¹³C]-bicarbonate production as a result of decrease PDH activity in a preclinical GBM model⁷⁴. Additionally, in a recent study, hyperpolarized [1-¹³C]-pyruvate was used as an imaging marker to monitor decreased expression of MCT1 (responsible primarily for pyruvate cellular influx) and MCT4 (responsible primarily for lactate cellular efflux) in immortalized normal human astrocytes (NHAs) harboring the IDH1 mutation as compared to the IDH1 wild-type NHAs⁵⁷.

Response to treatment was also studied using hyperpolarized [1-¹³C]-pyruvate in GBM. A decrease in hyperpolarized [1-¹³C]-lactate/[1-¹³C]-pyruvate ratio was correlated with a drop in LDHA expression and HIF-1 α activity in response to Everolimus, a first-generation mTOR inhibitor, and in response to LY294002, a PI3K inhibitor, in GS-2 GBM cells^{37,67} and in a GS-2 rat orthotopic tumor model⁷³. A similar observation was made following treatment with Voxelisib, a second-generation dual PI3K/mTOR inhibitor in GS-2 and U87 GBM models in mice⁷⁰. In response to treatment with Temozolomide (TMZ), the current standard of care for GBM, a decrease in pyruvate kinase M2 (PKM2) in orthotopic U87 and GS-2 GBM models in rats also led to a decrease in hyperpolarized [1-¹³C]-lactate production^{70,75,76}. Importantly, a drop in hyperpolarized [1-¹³C]-lactate production in all these models was an early event that occurred prior to tumor shrinkage and was associated with increased animal survival. Recently, treatment with dichloroacetate (DCA), a PDH activator, resulted in a drop in hyperpolarized [1-¹³C]-lactate/[¹³C]-bicarbonate ratio in rat C6 GBM⁷⁴. The [1-¹³C]-lactate/[1-¹³C]-pyruvate ratio was also used as an index of response to radiotherapy in C6 GBM⁷¹. Finally, one study reported the potential of hyperpolarized [1-¹³C]-pyruvate to evaluate response to the histone deacetylase inhibitor SAHA in a GBM cell model (GBM14), and, more importantly, to serve as a biomarker of acquired resistance to treatment⁶⁸. In contrast, in mutant IDH1 tumors, recent studies in our lab demonstrate that response to TMZ-treatment and tumor shrinkage did not lead to a detectable drop in hyperpolarized [1-¹³C]-lactate production⁶⁹.

[2-¹³C]-pyruvate

Recently, one study reported the first application of hyperpolarized [2-¹³C]-pyruvate in a rat C6 GBM model⁷⁷. Using a volumetric spiral chemical shift imaging method, reduced hyperpolarized [5-¹³C]-glutamate and increased [2-¹³C]-lactate were observed compared to normal brain. Upon DCA injection, these changes were reversed. Similarly, in models of mutant IDH1 cells, lower hyperpolarized [5-¹³C]-glutamate production following [2-¹³C]-pyruvate injection was observed in two genetically engineered cell models (U87 and NHAs) expressing the IDH1 mutation as compared to cells expressing wild-type IDH1 associated with a HIF-1 α -mediated decrease in PDH activity⁵⁸. In the same study, treatment with

DCA also resulted in an increase in hyperpolarized [5-¹³C]-glutamate. This points to one metabolic event that is similar in primary GBM and mutant IDH1 glioma cells.

Specific biomarker of IDH1 mutation: hyperpolarized [1-¹³C]-alpha ketoglutarate

As mentioned previously, the IDH1 mutation leads to elevated levels of 2-HG production. Monitoring IDH1 mutational status using hyperpolarized ¹³C MRS is therefore of great value. Recently, following the optimization of [1-¹³C]-α-KG as an hyperpolarized agent with sufficiently long T1 and adequate polarization (T1~52s at 3T and polarization level~16%^{30,78}), our group showed the accumulation of [1-¹³C]-2-HG (Figure 1) both *in vitro* and in an orthotopic preclinical model engineered to express mutant IDH1⁷⁸. Additionally, a drop in the conversion of [1-¹³C]-α-KG to [1-¹³C]-glutamate (Figure 1) was also detected in the same orthotopic glioma model and was correlated with a drop in the activity and expression of several enzymes (BCAT1, AST1/2, GDH1/2) that catalyze the α-KG to glutamate conversion, associated with their 2-HG-induced promoter methylation and silencing⁷⁹. *In vivo* detection of [1-¹³C]-α-KG conversion was possible thanks to a recently developed hyperpolarized ¹³C acquisition scheme that combines the use of a multiband spectral-spatial RF pulse sequence to optimize substrate and products excitations with a variable flip angle strategy⁶².

Other promising hyperpolarized probes

Other promising probes have been developed for the study of metabolism in physiological condition *in vitro* and *in vivo*^{28,30,80}. These have not yet been applied to brain tumor studies, but could be of interest (Figure 1).

[1-¹³C]-ethyl pyruvate

In hyperpolarized studies, time is a limiting factor. The faster the hyperpolarized agent can be delivered to the site of interest, the higher the SNR and chances of observing metabolic conversion. In studies of normal brain or low-grade glioma, where the BBB is not broken, agents must diffuse rapidly through the BBB. To respond to this constraint, Hurd et al. showed the advantage of using hyperpolarized [1-¹³C]-ethyl pyruvate (T1~45s at 3T and polarization level~28–35%), an analog of hyperpolarized [1-¹³C]-pyruvate that diffuses faster through the BBB⁸¹. This agent could potentially provide a better reading of tumor glycolysis. However, the requirement for an extra metabolic step, namely the conversion of ethyl pyruvate into pyruvate, prior to its subsequent metabolism, could limit the expected advantage of this probe.

[U-¹³C]-alpha-ketobutyrate

Another analog of pyruvate, alpha-ketobutyrate (α-KB), is also reduced by LDH but has a higher specificity towards LDHB, the enzyme that is typically responsible for the conversion of lactate into pyruvate (as opposed to pyruvate which has a higher specificity for LDHA)⁸². The conversion of hyperpolarized [U-¹³C]-α-KB (T1~52s at 3T and polarization level~10%) into [U-¹³C]-α-hydroxybutyrate was observed in the liver, heart and kidney of a

normal rat⁸². LDHB is highly expressed in the brain; therefore following changes in LDHB could be of great interest, particularly in low-grade tumors expressing the IDH1 mutation and wherein LDHA is silenced⁴².

[1-¹³C]-acetate

Acetate is a specific biomarker of glial metabolism as it is solely taken up by astrocytes. As such, several thermal studies of ¹³C-labeled acetate demonstrated the value of this metabolite in the study of normal brain metabolism^{83,84}. Additionally, the importance of acetate as a source to fuel tumor cells has recently been demonstrated in several studies^{50–52}. In the normal brain, the conversion of [1-¹³C]-acetate or [1,2-¹³C]-acetate (T1~40s at 9.4T and polarization level~9–17%) into [5-¹³C]- α -KG or [4,5-¹³C]- α -KG respectively was successfully detected using direct or polarization transfer detection techniques^{85,86}. However, studies in tumors have not been performed to date.

[1-¹³C]-dihydroascorbate

Redox balance in the tumor is correlated with aggressiveness and resistance to treatment^{59,87}. Redox reactions involve multiple agents, including glutathione, thioredoxin, NADPH, dehydroascorbic acid (DHA) and vitamin C, that are all implicated in controlling the level of ROS. Hyperpolarized [1-¹³C]-DHA has now been reported as a probe for imaging redox status (T1~57s at 3T and polarization level~6–8%)^{88,89}. The detection of the conversion of hyperpolarized [1-¹³C]-DHA into [1-¹³C]-vitamin C in normal rat brain as well as the modulation of this reaction in a model of prostate cancer illustrated the potential of this agent⁸⁸. DHA is transported into cells through the glucose transporter⁹⁰, making it a good candidate for *in vivo* brain studies and particularly interesting for the study of mutant IDH1 tumors wherein redox status is likely altered.

[5-¹³C]-glutamine

[5-¹³C]-glutamine is of interest in brain cancer metabolism due to the aforementioned importance of Myc in high-grade GBM. However, studies of the conversion of hyperpolarized [5-¹³C]-glutamine into [5-¹³C]-glutamate have been limited due to the short T1 of this substrate (T1~8s at 3T and polarization level~28%), the rapid degradation of glutamine into glutamate, which is also the metabolic product of interest, and the apparently slow uptake of glutamine by cells^{91–94}. Currently, three studies performed on hepatoma cells and prostate cancer cells, and one *in vivo* study performed in a rat model of liver cancer, reported the use of hyperpolarized glutamine^{91–94} but no other studies have been successful in using this compound.

[¹³C]-bicarbonate

As aforementioned, acidification of the extracellular environment plays an important role in tumor development. Rapid exchange between bicarbonate and carbon dioxide depends upon pH. Therefore, monitoring the fate of hyperpolarized [¹³C]-bicarbonate allows mapping of the extracellular pH (pHe) and studies in murine lymphoma⁹⁵ or prostate cancer⁹⁶ models reported the use of hyperpolarized [¹³C]-bicarbonate (T1~10s at 9.4T and polarization level~16%) to image pHe. More recently, a new pH probe, [1-¹³C]-1,2-glycerol carbonate

was developed and was used in a prostate cancer model⁹⁷. These probes could therefore be used to monitor pH in brain tumors, where the extracellular pH is likely acidic in GBM, but likely not in the case of mutant IDH-driven tumors that have silence LDH-A and reduced lactate production^{42,69}.

[1,4-¹³C₂]-fumarate

Increased permeability of necrotic cell plasma membrane within the tumor facilitates the entry of fumarate within necrotic cells or release of the fumarase enzyme within the tumor microenvironment, resulting in increased conversion of fumarate, an intermediate of the TCA cycle, into malate. In contrast, in normal cells where the integrity of the plasma membrane has not been compromised, the entry of fumarate is limited over the lifetime of the hyperpolarized probe. Hyperpolarized [1,4-¹³C₂]-fumarate (T1~24s at 9.4T and polarization level~26–35%) has been used to monitor treatment response *in vivo* in an implanted EL-4 murine lymphoma^{98,99} and human breast adenocarcinoma¹⁰⁰. To date, no studies of hyperpolarized [1,4-¹³C₂]-fumarate have reported in brain tumors. However, in the case of GBM, where the entry of fumarate is facilitated by the disruption of the BBB, hyperpolarized [1,4-¹³C₂]-fumarate could potentially detect cell death.

[2-¹³C, 1,2-²H₄]-choline chloride

Monitoring choline metabolism in high- and low-grade gliomas is of significant interest due to their abnormal choline metabolism. A recent study showed that [2-¹³C, 1,2-²H₄]-choline chloride can be hyperpolarized, fulfills the technical requirements for hyperpolarized studies (T1~60s at 7T and polarization level~28–35%) and its conversion into [2-¹³C, 1,2-²H₄]-acetylcholine can be detected in an *in vitro* acetyltransferase enzyme experiment^{101,102}. *In vivo*, distribution of the hyperpolarized substrate was observed in the inferior vena cava, heart, aorta and kidneys¹⁰³. However, metabolism into PC has not been reported to date in cells or *in vivo*.

Hyperpolarized [¹³C]-urea: beyond metabolism, probing brain tumor perfusion

In addition to tumor metabolism, measuring tumor vascularity and perfusion provide crucial information to monitor tumor evolution and response to treatment. Hyperpolarized [¹³C]-urea has been well studied in the context of prostate, liver and kidney cancers^{104–106}. However, permeability of brain tissue to urea is very low limiting its application to the study of brain perfusion¹⁰⁷. Recently, two novel hyperpolarized agents were developed, [¹³C]-hydroxymethyl cyclopropane (HMCP) and [¹³C]-t-butanol, with the latest diffusing freely into normal brain tissue¹⁰⁷. In a recent study, [¹³C]-HMCP was used to investigate tumor perfusion in an orthotopic human glioblastoma model (G55 MG)¹⁰⁸. The strong correlation between hyperpolarized findings, conventional perfusion imaging and level of vascular staining detected by immunohistochemistry illustrates the potential of this new agent.

Conclusion

Over the past decade, studies using the dissolution DNP method combined with ^{13}C MRS have demonstrated the potential of this technique to change the future of brain cancer diagnosis. By enhancing the signal from ^{13}C -labeled compounds, this new metabolic imaging approach enables probing in real-time, non-invasively, and in a non-ionizing manner, major metabolic pathways and their reprogramming in cancer. So far, several agents have been developed to target different pathways and monitor response to therapies, and more will likely emerge in the years to come. Importantly, the potential of this technique is not limited to the study of brain tumors but is applicable to many other cancers and diseases³⁰. Finally, the recent first-in-human study performed on prostate cancer patient²⁹ as well as the beginning of a clinical trial in brain tumor patients at the University of California, San Francisco, confirms the potential of this technique for translation to the clinic.

Acknowledgments

Financial Support

This work was supported by NIH R01CA172845, NIH R21CA201453, NIH R01CA1972254 and the UCSF Brain Tumor Center Loglio Collective.

References

1. Ostrom QT, et al. CBTRUS Statistical Report: Primary Brain and Central Nervous System Tumors Diagnosed in the United States in 2008–2012. *Neuro-oncology*. 2015; 17(Suppl 4):iv1–iv62. [PubMed: 26511214]
2. Huse JT, Phillips HS, Brennan CW. Molecular subclassification of diffuse gliomas: seeing order in the chaos. *Glia*. 2011; 59:1190–1199. [PubMed: 21446051]
3. Ohgaki H, Kleihues P. The definition of primary and secondary glioblastoma. *Clinical cancer research : an official journal of the American Association for Cancer Research*. 2013; 19:764–772. [PubMed: 23209033]
4. Ohgaki H, Kleihues P. Genetic pathways to primary and secondary glioblastoma. *The American journal of pathology*. 2007; 170:1445–1453. [PubMed: 17456751]
5. Cancer Genome Atlas Research N. Comprehensive genomic characterization defines human glioblastoma genes and core pathways. *Nature*. 2008; 455:1061–1068. [PubMed: 18772890]
6. Izquierdo-Garcia JL, et al. Glioma cells with the IDH1 mutation modulate metabolic fractional flux through pyruvate carboxylase. *PLoS one*. 2014; 9:e108289. [PubMed: 25243911]
7. Viswanath P, Chaumeil MM, Ronen SM. Molecular Imaging of Metabolic Reprogramming in Mutant IDH Cells. *Frontiers in oncology*. 2016; 6:60. [PubMed: 27014635]
8. Parsons DW, et al. An integrated genomic analysis of human glioblastoma multiforme. *Science*. 2008; 321:1807–1812. [PubMed: 18772396]
9. Cohen AL, Holmen SL, Colman H. IDH1 and IDH2 mutations in gliomas. *Current neurology and neuroscience reports*. 2013; 13:345. [PubMed: 23532369]
10. Prensner JR, Chinnaiyan AM. Metabolism unhinged: IDH mutations in cancer. *Nature medicine*. 2011; 17:291–293.
11. Ichimura K, et al. IDH1 mutations are present in the majority of common adult gliomas but rare in primary glioblastomas. *Neuro-oncology*. 2009; 11:341–347. [PubMed: 19435942]
12. Cha S. Update on brain tumor imaging: from anatomy to physiology. *AJNR. American journal of neuroradiology*. 2006; 27:475–487. [PubMed: 16551981]

13. Chaumeil MM, Lupo JM, Ronen SM. Magnetic Resonance (MR) Metabolic Imaging in Glioma. *Brain pathology*. 2015; 25:769–780. [PubMed: 26526945]
14. Ryken TC, et al. The role of imaging in the management of progressive glioblastoma : a systematic review and evidence-based clinical practice guideline. *Journal of neuro-oncology*. 2014; 118:435–460. [PubMed: 24715656]
15. Gillies RJ, Morse DL. In vivo magnetic resonance spectroscopy in cancer. *Annual review of biomedical engineering*. 2005; 7:287–326.
16. van der Graaf M. In vivo magnetic resonance spectroscopy: basic methodology and clinical applications. *European biophysics journal : EBJ*. 2010; 39:527–540. [PubMed: 19680645]
17. Horska A, Barker PB. Imaging of brain tumors: MR spectroscopy and metabolic imaging. *Neuroimaging clinics of North America*. 2010; 20:293–310. [PubMed: 20708548]
18. Li Y, Park I, Nelson SJ. Imaging tumor metabolism using in vivo magnetic resonance spectroscopy. *Cancer journal*. 2015; 21:123–128.
19. Elkhaled A, et al. Characterization of metabolites in infiltrating gliomas using ex vivo (1)H high-resolution magic angle spinning spectroscopy. *NMR in biomedicine*. 2014; 27:578–593. [PubMed: 24596146]
20. Pope WB, et al. Non-invasive detection of 2-hydroxyglutarate and other metabolites in IDH1 mutant glioma patients using magnetic resonance spectroscopy. *Journal of neuro-oncology*. 2012; 107:197–205. [PubMed: 22015945]
21. Andronesi OC, et al. Detection of 2-hydroxyglutarate in IDH-mutated glioma patients by in vivo spectral-editing and 2D correlation magnetic resonance spectroscopy. *Science translational medicine*. 2012; 4:116ra114.
22. Choi C, et al. 2-hydroxyglutarate detection by magnetic resonance spectroscopy in IDH-mutated patients with gliomas. *Nature medicine*. 2012; 18:624–629.
23. Emir UE, et al. Noninvasive Quantification of 2-Hydroxyglutarate in Human Gliomas with IDH1 and IDH2 Mutations. *Cancer research*. 2016; 76:43–49. [PubMed: 26669865]
24. Elkhaled A, et al. Magnetic resonance of 2-hydroxyglutarate in IDH1-mutated low-grade gliomas. *Science translational medicine*. 2012; 4:116ra115.
25. Kalinina J, et al. Detection of “oncometabolite” 2-hydroxyglutarate by magnetic resonance analysis as a biomarker of IDH1/2 mutations in glioma. *Journal of molecular medicine*. 2012; 90:1161–1171. [PubMed: 22426639]
26. Maher EA, et al. Metabolism of [U-13 C]glucose in human brain tumors in vivo. *NMR in biomedicine*. 2012; 25:1234–1244. [PubMed: 22419606]
27. Ardenkjaer-Larsen JH, et al. Increase in signal-to-noise ratio of > 10,000 times in liquid-state NMR. *Proceedings of the National Academy of Sciences of the United States of America*. 2003; 100:10158–10163. [PubMed: 12930897]
28. Kurhanewicz J, et al. Analysis of cancer metabolism by imaging hyperpolarized nuclei: prospects for translation to clinical research. *Neoplasia*. 2011; 13:81–97. [PubMed: 21403835]
29. Nelson SJ, et al. Metabolic imaging of patients with prostate cancer using hyperpolarized [1-(1)(3)C]pyruvate. *Science translational medicine*. 2013; 5:198ra108.
30. Chaumeil MM, Najac C, Ronen SM. Studies of Metabolism Using (13)C MRS of Hyperpolarized Probes. *Methods in enzymology*. 2015; 561:1–71. [PubMed: 26358901]
31. Warburg O. On the origin of cancer cells. *Science*. 1956; 123:309–314. [PubMed: 13298683]
32. Ward PS, Thompson CB. Metabolic reprogramming: a cancer hallmark even warburg did not anticipate. *Cancer cell*. 2012; 21:297–308. [PubMed: 22439925]
33. Gatenby RA, Gillies RJ. Why do cancers have high aerobic glycolysis? *Nature reviews. Cancer*. 2004; 4:891–899. [PubMed: 15516961]
34. Lunt SY, Vander Heiden MG. Aerobic glycolysis: meeting the metabolic requirements of cell proliferation. *Annual review of cell and developmental biology*. 2011; 27:441–464.
35. Vander Heiden MG, Cantley LC, Thompson CB. Understanding the Warburg effect: the metabolic requirements of cell proliferation. *Science*. 2009; 324:1029–1033. [PubMed: 19460998]
36. Hanahan D, Weinberg RA. Hallmarks of cancer: the next generation. *Cell*. 2011; 144:646–674. [PubMed: 21376230]

37. Venkatesh HS, et al. Reduced phosphocholine and hyperpolarized lactate provide magnetic resonance biomarkers of PI3K/Akt/mTOR inhibition in glioblastoma. *Neuro-oncology*. 2012; 14:315–325. [PubMed: 22156546]
38. Rodon J, Dienstmann R, Serra V, Tabernero J. Development of PI3K inhibitors: lessons learned from early clinical trials. *Nature reviews. Clinical oncology*. 2013; 10:143–153.
39. Doherty JR, Cleveland JL. Targeting lactate metabolism for cancer therapeutics. *The Journal of clinical investigation*. 2013; 123:3685–3692. [PubMed: 23999443]
40. Pinheiro C, et al. Role of monocarboxylate transporters in human cancers: state of the art. *Journal of bioenergetics and biomembranes*. 2012; 44:127–139. [PubMed: 22407107]
41. Rabow L, Kristensson K. Changes in lactate dehydrogenase isoenzyme patterns in patients with tumours of the central nervous system? *Acta neurochirurgica*. 1977; 36:71–81. [PubMed: 835389]
42. Chesnelong C, et al. Lactate dehydrogenase A silencing in IDH mutant gliomas. *Neuro-oncology*. 2014; 16:686–695. [PubMed: 24366912]
43. Glunde K, Bhujwala ZM, Ronen SM. Choline metabolism in malignant transformation. *Nature reviews. Cancer*. 2011; 11:835–848. [PubMed: 22089420]
44. Righi V, et al. 1H HR-MAS and genomic analysis of human tumor biopsies discriminate between high and low grade astrocytomas. *NMR in biomedicine*. 2009; 22:629–637. [PubMed: 19322812]
45. Glunde K, Jacobs MA, Bhujwala ZM. Choline metabolism in cancer: implications for diagnosis and therapy. *Expert review of molecular diagnostics*. 2006; 6:821–829. [PubMed: 17140369]
46. Herms JW, von Loewenich FD, Behnke J, Markakis E, Kretzschmar HA. c-myc oncogene family expression in glioblastoma and survival. *Surgical neurology*. 1999; 51:536–542. [PubMed: 10321885]
47. Annibali D, et al. Myc inhibition is effective against glioma and reveals a role for Myc in proficient mitosis. *Nature communications*. 2014; 5:4632.
48. Hensley CT, Wasti AT, DeBerardinis RJ. Glutamine and cancer: cell biology, physiology, and clinical opportunities. *The Journal of clinical investigation*. 2013; 123:3678–3684. [PubMed: 23999442]
49. DeBerardinis RJ, et al. Beyond aerobic glycolysis: transformed cells can engage in glutamine metabolism that exceeds the requirement for protein and nucleotide synthesis. *Proceedings of the National Academy of Sciences of the United States of America*. 2007; 104:19345–19350. [PubMed: 18032601]
50. Mashimo T, et al. Acetate is a bioenergetic substrate for human glioblastoma and brain metastases. *Cell*. 2014; 159:1603–1614. [PubMed: 25525878]
51. Comerford SA, et al. Acetate dependence of tumors. *Cell*. 2014; 159:1591–1602. [PubMed: 25525877]
52. Kamphorst JJ, Chung MK, Fan J, Rabinowitz JD. Quantitative analysis of acetyl-CoA production in hypoxic cancer cells reveals substantial contribution from acetate. *Cancer & metabolism*. 2014; 2:23. [PubMed: 25671109]
53. Esmaeili M, et al. IDH1 R132H mutation generates a distinct phospholipid metabolite profile in glioma. *Cancer research*. 2014; 74:4898–4907. [PubMed: 25005896]
54. Izquierdo-Garcia JL, et al. Metabolic reprogramming in mutant IDH1 glioma cells. *PloS one*. 2015; 10:e0118781. [PubMed: 25706986]
55. Reitman ZJ, et al. Profiling the effects of isocitrate dehydrogenase 1 and 2 mutations on the cellular metabolome. *Proceedings of the National Academy of Sciences of the United States of America*. 2011; 108:3270–3275. [PubMed: 21289278]
56. Mayers JR, Vander Heiden MG. BCAT1 defines gliomas by IDH status. *Nature medicine*. 2013; 19:816–817.
57. Viswanath P, et al. Mutant IDH1 expression is associated with down-regulation of monocarboxylate transporters. *Oncotarget*. 2016
58. Izquierdo-Garcia JL, et al. IDH1 Mutation Induces Reprogramming of Pyruvate Metabolism. *Cancer research*. 2015; 75:2999–3009. [PubMed: 26045167]

59. Shi J, et al. Decreasing GSH and increasing ROS in chemosensitivity gliomas with IDH1 mutation. *Tumour biology : the journal of the International Society for Oncodevelopmental Biology and Medicine*. 2015; 36:655–662. [PubMed: 25283382]
60. Hurd RE, Yen YF, Chen A, Ardenkjaer-Larsen JH. Hyperpolarized ^{13}C metabolic imaging using dissolution dynamic nuclear polarization. *Journal of magnetic resonance imaging : JMRI*. 2012; 36:1314–1328. [PubMed: 23165733]
61. Kerr, AB., et al. Multiband spectral-spatial design for high-field and hyperpolarized C-13 applications. *Proceedings of the 16th Annual Meeting of ISMRM; Toronto*. 2008. p. 226
62. Larson PE, et al. Multiband excitation pulses for hyperpolarized ^{13}C dynamic chemical-shift imaging. *Journal of magnetic resonance*. 2008; 194:121–127. [PubMed: 18619875]
63. Larson PE, Kerr AB, Swisher CL, Pauly JM, Vigneron DB. A rapid method for direct detection of metabolic conversion and magnetization exchange with application to hyperpolarized substrates. *Journal of magnetic resonance*. 2012; 225:71–80. [PubMed: 23143011]
64. von Morze C, et al. Frequency-specific SSFP for hyperpolarized $(1)(3)\text{C}$ metabolic imaging at 14.1 T. *Magnetic resonance imaging*. 2013; 31:163–170. [PubMed: 22898680]
65. Xing Y, Reed GD, Pauly JM, Kerr AB, Larson PE. Optimal variable flip angle schemes for dynamic acquisition of exchanging hyperpolarized substrates. *Journal of magnetic resonance*. 2013; 234:75–81. [PubMed: 23845910]
66. Golman K, in 't Zandt R, Thaning M. Real-time metabolic imaging. *Proceedings of the National Academy of Sciences of the United States of America*. 2006; 103:11270–11275. [PubMed: 16837573]
67. Ward CS, et al. Noninvasive detection of target modulation following phosphatidylinositol 3-kinase inhibition using hyperpolarized ^{13}C magnetic resonance spectroscopy. *Cancer research*. 2010; 70:1296–1305. [PubMed: 20145128]
68. Eriksson P, Chaumeil MM, Mukherjee J, Pieper RO, Ronen SM. ^{13}C MRS of hyperpolarized [1- ^{13}C] pyruvate can differentiate between SAHA resistant and sensitive glioblastoma cells. in. *Proc Int Soc Magn Reson Med*. 2015; 74
69. Chaumeil MM, et al. Hyperpolarized $(13)\text{C}$ MR imaging detects no lactate production in mutant IDH1 gliomas: Implications for diagnosis and response monitoring. *NeuroImage. Clinical*. 2016; 12:180–189. [PubMed: 27437179]
70. Radoul M, et al. MR Studies of Glioblastoma Models Treated with Dual PI3K/mTOR Inhibitor and Temozolomide - Metabolic Changes are Associated with Enhanced Survival. *Molecular cancer therapeutics*. 2016
71. Day SE, et al. Detecting response of rat C6 glioma tumors to radiotherapy using hyperpolarized [1- ^{13}C]pyruvate and ^{13}C magnetic resonance spectroscopic imaging. *Magnetic resonance in medicine : official journal of the Society of Magnetic Resonance in Medicine / Society of Magnetic Resonance in Medicine*. 2011; 65:557–563.
72. Park I, et al. Hyperpolarized ^{13}C magnetic resonance metabolic imaging: application to brain tumors. *Neuro-oncology*. 2010; 12:133–144. [PubMed: 20150380]
73. Chaumeil MM, et al. Hyperpolarized ^{13}C MR spectroscopic imaging can be used to monitor Everolimus treatment in vivo in an orthotopic rodent model of glioblastoma. *NeuroImage*. 2012; 59:193–201. [PubMed: 21807103]
74. Park JM, et al. Metabolic response of glioma to dichloroacetate measured in vivo by hyperpolarized $(13)\text{C}$ magnetic resonance spectroscopic imaging. *Neuro-oncology*. 2013; 15:433–441. [PubMed: 23328814]
75. Park I, et al. Detection of early response to temozolomide treatment in brain tumors using hyperpolarized ^{13}C MR metabolic imaging. *Journal of magnetic resonance imaging : JMRI*. 2011; 33:1284–1290. [PubMed: 21590996]
76. Park I, et al. Changes in pyruvate metabolism detected by magnetic resonance imaging are linked to DNA damage and serve as a sensor of temozolomide response in glioblastoma cells. *Cancer research*. 2014; 74:7115–7124. [PubMed: 25320009]
77. Park JM, et al. Volumetric spiral chemical shift imaging of hyperpolarized [2-(^{13}C)]pyruvate in a rat c6 glioma model. *Magnetic resonance in medicine : official journal of the Society of Magnetic Resonance in Medicine / Society of Magnetic Resonance in Medicine*. 2016; 75:973–984.

78. Chaumeil MM, et al. Non-invasive in vivo assessment of IDH1 mutational status in glioma. *Nature communications*. 2013; 4:2429.
79. Chaumeil MM, et al. Hyperpolarized [1-13C] glutamate: a metabolic imaging biomarker of IDH1 mutational status in glioma. *Cancer research*. 2014; 74:4247–4257. [PubMed: 24876103]
80. Keshari KR, Wilson DA. Chemistry and biochemistry of 13C hyperpolarized magnetic resonance using dynamic nuclear polarization. *Chemical Society Reviews*. 2014; 43:1627–1659. [PubMed: 24363044]
81. Hurd RE, et al. Metabolic imaging in the anesthetized rat brain using hyperpolarized [1-13C] pyruvate and [1-13C] ethyl pyruvate. *Magnetic resonance in medicine : official journal of the Society of Magnetic Resonance in Medicine / Society of Magnetic Resonance in Medicine*. 2010; 63:1137–1143.
82. von Morze C, et al. Hyperpolarized [(13) C]ketobutyrate, a molecular analog of pyruvate with modified specificity for LDH isoforms. *Magnetic resonance in medicine : official journal of the Society of Magnetic Resonance in Medicine / Society of Magnetic Resonance in Medicine*. 2016; 75:1894–1900.
83. Deelchand DK, Shestov AA, Koski DM, Ugurbil K, Henry PG. Acetate transport and utilization in the rat brain. *Journal of neurochemistry*. 2009; 109(Suppl 1):46–54. [PubMed: 19393008]
84. Lebon V, et al. Astroglial contribution to brain energy metabolism in humans revealed by 13C nuclear magnetic resonance spectroscopy: elucidation of the dominant pathway for neurotransmitter glutamate repletion and measurement of astrocytic oxidative metabolism. *The Journal of neuroscience : the official journal of the Society for Neuroscience*. 2002; 22:1523–1531. [PubMed: 11880482]
85. Mishkovsky M, Comment A, Gruetter R. In vivo detection of brain Krebs cycle intermediate by hyperpolarized magnetic resonance. *Journal of cerebral blood flow and metabolism : official journal of the International Society of Cerebral Blood Flow and Metabolism*. 2012; 32:2108–2113.
86. Comment A, et al. Producing over 100 ml of highly concentrated hyperpolarized solution by means of dissolution DNP. *Journal of magnetic resonance*. 2008; 194:152–155. [PubMed: 18595751]
87. Wallace DC. Mitochondria and cancer. *Nature reviews. Cancer*. 2012; 12:685–698. [PubMed: 23001348]
88. Keshari KR, et al. Hyperpolarized 13C dehydroascorbate as an endogenous redox sensor for in vivo metabolic imaging. *Proceedings of the National Academy of Sciences of the United States of America*. 2011; 108:18606–18611. [PubMed: 22042839]
89. Bohndiek SE, et al. Hyperpolarized [1-13C]-ascorbic and dehydroascorbic acid: vitamin C as a probe for imaging redox status in vivo. *Journal of the American Chemical Society*. 2011; 133:11795–11801. [PubMed: 21692446]
90. Kc S, Carcamo JM, Golde DW. Vitamin C enters mitochondria via facilitative glucose transporter 1 (Glut1) and confers mitochondrial protection against oxidative injury. *FASEB journal : official publication of the Federation of American Societies for Experimental Biology*. 2005; 19:1657–1667. [PubMed: 16195374]
91. Gallagher FA, Kettunen MI, Day SE, Lerche M, Brindle KM. 13C MR spectroscopy measurements of glutaminase activity in human hepatocellular carcinoma cells using hyperpolarized 13C-labeled glutamine. *Magnetic resonance in medicine : official journal of the Society of Magnetic Resonance in Medicine / Society of Magnetic Resonance in Medicine*. 2008; 60:253–257.
92. Dafni H, et al. Hyperpolarized 13C spectroscopic imaging informs on hypoxia-inducible factor-1 and myc activity downstream of platelet-derived growth factor receptor. *Cancer research*. 2010; 70:7400–7410. [PubMed: 20858719]
93. Canape C, et al. Probing treatment response of glutaminolytic prostate cancer cells to natural drugs with hyperpolarized [5-(13) C]glutamine. *Magnetic resonance in medicine : official journal of the Society of Magnetic Resonance in Medicine / Society of Magnetic Resonance in Medicine*. 2015; 73:2296–2305.
94. Cabella C, et al. In vivo and in vitro liver cancer metabolism observed with hyperpolarized [5-(13)C]glutamine. *Journal of magnetic resonance*. 2013; 232:45–52. [PubMed: 23689113]
95. Gallagher FA, et al. Magnetic resonance imaging of pH in vivo using hyperpolarized 13C-labelled bicarbonate. *Nature*. 2008; 453:940–943. [PubMed: 18509335]

96. Wilson DM, et al. Multi-compound polarization by DNP allows simultaneous assessment of multiple enzymatic activities in vivo. *Journal of magnetic resonance*. 2010; 205:141–147. [PubMed: 20478721]
97. Korenchan DE, et al. Dynamic nuclear polarization of biocompatible (13)C-enriched carbonates for in vivo pH imaging. *Chemical communications*. 2016; 52:3030–3033. [PubMed: 26792559]
98. Gallagher FA, et al. Production of hyperpolarized [1,4-13C2]malate from [1,4-13C2]fumarate is a marker of cell necrosis and treatment response in tumors. *Proceedings of the National Academy of Sciences of the United States of America*. 2009; 106:19801–19806. [PubMed: 19903889]
99. Bohndiek SE, et al. Detection of tumor response to a vascular disrupting agent by hyperpolarized 13C magnetic resonance spectroscopy. *Molecular cancer therapeutics*. 2010; 9:3278–3288. [PubMed: 21159611]
100. Witney TH, et al. Detecting treatment response in a model of human breast adenocarcinoma using hyperpolarised [1-13C]pyruvate and [1,4-13C2]fumarate. *British journal of cancer*. 2010; 103:1400–1406. [PubMed: 20924379]
101. Allouche-Arnon H, et al. A hyperpolarized choline molecular probe for monitoring acetylcholine synthesis. *Contrast media & molecular imaging*. 2011; 6:139–147. [PubMed: 21698772]
102. Allouche-Arnon H, Lerche MH, Karlsson M, Lenkinski RE, Katz-Brull R. Deuteration of a molecular probe for DNP hyperpolarization—a new approach and validation for choline chloride. *Contrast media & molecular imaging*. 2011; 6:499–506. [PubMed: 22144028]
103. Allouche-Arnon H, et al. In vivo magnetic resonance imaging of glucose - initial experience. *Contrast media & molecular imaging*. 2013; 8:72–82. [PubMed: 23109395]
104. Bahrami N, Swisher CL, Von Morze C, Vigneron DB, Larson PE. Kinetic and perfusion modeling of hyperpolarized (13)C pyruvate and urea in cancer with arbitrary RF flip angles. *Quantitative imaging in medicine and surgery*. 2014; 4:24–32. [PubMed: 24649432]
105. von Morze C, et al. Imaging of blood flow using hyperpolarized [(13)C]urea in preclinical cancer models. *Journal of magnetic resonance imaging : JMRI*. 2011; 33:692–697. [PubMed: 21563254]
106. von Morze C, et al. Investigating tumor perfusion and metabolism using multiple hyperpolarized (13)C compounds: HP001, pyruvate and urea. *Magnetic resonance imaging*. 2012; 30:305–311. [PubMed: 22169407]
107. von Morze C, et al. Simultaneous multiagent hyperpolarized (13)C perfusion imaging. *Magnetic resonance in medicine : official journal of the Society of Magnetic Resonance in Medicine / Society of Magnetic Resonance in Medicine*. 2014; 72:1599–1609.
108. Park I, et al. Investigating tumor perfusion by hyperpolarized C MRI with comparison to conventional gadolinium contrast-enhanced MRI and pathology in orthotopic human GBM xenografts. *Magnetic resonance in medicine : official journal of the Society of Magnetic Resonance in Medicine / Society of Magnetic Resonance in Medicine*. 2016

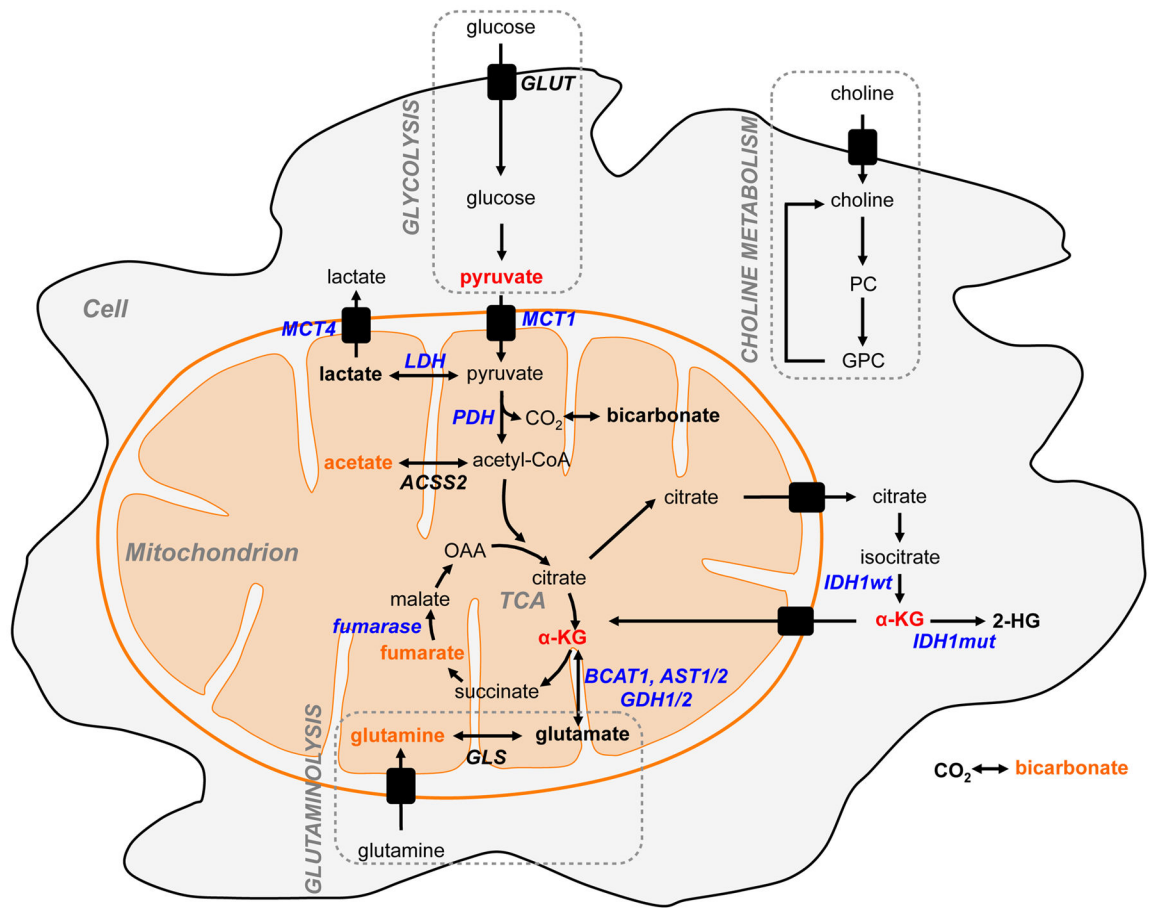


Figure 1. Illustration of the metabolic pathways with their associated DNP probes applied to the study of GBM and low-grade mutant IDH1 glioma (red) and potential future probes (orange).

Table 1

List of ¹³C DNP probes that have been polarized and MR sequences applied to the study of altered metabolic pathways in orthotopic GBM model and cells.

Altered Pathways	HP ¹³ C MRS			REF
	HP Probe	Sequences	Use	
<ul style="list-style-type: none"> Pyruvate metabolism through activation of PI3K/Akt/mTORC1 and stabilization of HIF1-α: <ul style="list-style-type: none"> ✓ ↑ glucose transporter ✓ ↑ glycolysis ✓ ↑ PDK1 enzyme ✓ ↓ PDH activity ✓ ↑ LDHA ✓ ↑ MCTs 	[1,1-¹³C]-pyruvate T1-67s at 3T P _{hpr} -14-40%	<ul style="list-style-type: none"> • 	<ul style="list-style-type: none"> • dynamic and single time point 2D CSI with low flip angle single time point 2D MR spectroscopic imaging using double spin echo RF pulse with variable flip angle dynamic non localized acquisition with low flip angle	31, 32, 39, 40 37, 57, 66-76
	[2,1-¹³C]-pyruvate T1-40s at 3T P _{hpr} -27%	<ul style="list-style-type: none"> • 	<ul style="list-style-type: none"> • Conversion to [1,1- ¹³ C]-lactate ✓ ↑ in several preclinical orthotopic GBM models (GS-2, U87, c6 glioma) ✓ ↓ after treatment with Everolimus, LY294002, Voxelator, Temozolomide, DCA (in GS-2, U87, c6 glioma models) Conversion to [1,3- ¹³ C]-bicarbonate: ✓ ↓ in rat c6 glioblastoma model ✓ ↑ with DCA treatment in rat c6 glioma model	30, 77
Primary GBM	[2,1-¹³C]-pyruvate T1-40s at 3T P _{hpr} -27%	<ul style="list-style-type: none"> • 	<ul style="list-style-type: none"> • Conversion to [2,1- ¹³ C]-lactate ✓ ↑ in rat c6 glioma model ✓ ↓ following DCA treatment in same model Conversion to [5,1- ¹³ C]-glutamate ✓ ↓ in rat c6 glioma model ✓ ↑ following DCA treatment in same model	81
	[1,1-¹³C]-ethyl pyruvate T1-45s at 3T P _{hpr} -28-35%	<ul style="list-style-type: none"> • 	<ul style="list-style-type: none"> • Not yet applied to the study of GBM	82
	[U,1-¹³C]-α-KB T1-52s at 3T P _{hpr} -10%	<ul style="list-style-type: none"> • 	<ul style="list-style-type: none"> • Not yet applied to the study of GBM	91-94
	[5,1-¹³C]-glutamine T1-88s at 3T P _{hpr} -28%	<ul style="list-style-type: none"> • 	<ul style="list-style-type: none"> • Not yet applied to the study of GBM: rapid degradation into two by-products, low glutamine uptake by cells and short T1	101-103
	[2,1-¹³C, 1,2-²H]-choline chloride T1-60s at 3T P _{hpr} -28-35%	<ul style="list-style-type: none"> • 	<ul style="list-style-type: none"> • Not yet applied to the study of GBM	43-45
	Glutamine metabolism by an increase of Myc activity <ul style="list-style-type: none"> ✓ ↑ glutaminase 	<ul style="list-style-type: none"> • 	<ul style="list-style-type: none"> • Abnormal choline metabolism through activation of PI3K/Akt/mTORC1 and stabilization of HIF1-α: ✓ ↑ PC ✓ ↓ GPC	32, 46-49

Altered Pathways	REF	HP Probe	Sequences	Use	REF
<ul style="list-style-type: none"> • <i>Acidification of the extracellular microenvironment</i> <ul style="list-style-type: none"> ✓ ↑ glucose transporter ✓ ↑ glycolysis ✓ ↑ MCTs 	33,40	<i>[1-13C]-bicarbonate</i> T1 ~10s at 9.4T P _{hip} ~16%		•	95-97
<ul style="list-style-type: none"> • <i>Necrosis: increase permeability of the necrotic cell membrane</i> <ul style="list-style-type: none"> ✓ ↑ uptake fumarate ✓ ↑ release fumarase enzyme 	98-100	<i>[1,4-13C2]fumarate</i> T1 ~24s at 9.4T P _{hip} ~26-35%		•	98-100
<ul style="list-style-type: none"> • <i>Increased acetate uptake</i> <ul style="list-style-type: none"> ✓ ↑ acetyl-CoA synthase enzyme 2 	50-52	<i>[1-13C]-acetate and [2-13C]-acetate</i> T1 ~40s at 9.4T P _{hip} ~9-17%		<ul style="list-style-type: none"> • <i>In vivo:</i> ✓ • direct or polarization transfer detection technique 	85

List of ¹³C DNP probes that have been polarized and MR sequences applied to the study of altered metabolic pathways in low-grade mutant IDH1 glioma orthotopic model and cells.

Table 2

Altered Pathways	HP ¹³ C MRS			
	HP Probe	Sequences	Use	REF
<ul style="list-style-type: none"> Alterations linked to 2-HG accumulation ✓ ↑ 2-HG ✓ ↓ BCAT1, AST1/2, GDH1/2 activities ✓ LDHA silencing ✓ ↓ PDH ✓ ↓ MCT1 and MCT4 	<p><i>[1-¹³C]-α-KG</i> T1-52s at 9.4T P_{hp}-16%</p>	<p><i>In vivo:</i> ✓</p> <p><i>In cells:</i> ✓</p>	<ul style="list-style-type: none"> • Multiband spectral-spatial RF pulse with variable flip angle • dynamic non localized acquisition with low flip angle 	<p>62, 78, 79</p> <p><i>Conversion to [1-¹³C]-2-HG: ↑ both in cells and in an orthotopic glioma model harboring IDH1 mutation</i> <i>Conversion to [1-¹³C]-glutamate: ↓ in an orthotopic U87 glioma harboring IDH1 mutation</i></p>
	<p><i>[1-¹³C]-pyruvate</i> T1-67s at 3T P_{hp}-14-40%</p>	<p><i>In vivo:</i> ✓</p> <p><i>In cells:</i> ✓</p>	<ul style="list-style-type: none"> • dynamic 2D CSI with low flip angle • dynamic non localized acquisition with low flip angle 	<p>69, 57</p> <p><i>Conversion to [1-¹³C]-lactate:</i> ✓ low production in an orthotopic tumor model ✓ ↓ in cells harboring IDH1 mutation as compared to the IDH1 wild-type cells</p>
<p>Low-grade mutant IDH1 glioma</p>	<p><i>[2-¹³C]-pyruvate</i> T1-40s at 3T P_{hp}-27%</p>	<p><i>In cells:</i> ✓</p>	<ul style="list-style-type: none"> • dynamic non localized acquisition with low flip angle 	<p>30, 77</p> <p><i>Conversion to [2-¹³C]-lactate</i> ✓ ↑ in U87 and NHAAs cells ✓ ↓ following DCA treatment in same cell models <i>Conversion to [5-¹³C]-glutamate</i> ✓ ↓ in U87 and NHAAs cells ✓ ↑ following DCA treatment in same cell models</p>
	<p><i>[1-¹³C]-α-ketoglutarate</i> T1-45s at 3T P_{hp}-28-35%</p>			<p>81</p> <p>Not yet applied to the study of low-grade brain tumor</p>
	<p><i>[U-¹³C]-α-KB</i> T1-52s at 3T P_{hp}-10%</p>			<p>82</p> <p>Not yet applied to the study of low-grade brain tumor</p>
<ul style="list-style-type: none"> Elevated levels of ROS linked to reduce activity of wild-type IDH1 ✓ ↓ NADPH 	<p><i>[1-¹³C]-α-ketoglutarate</i> T1-57s at 3T P_{hp}-6-8%</p>			<p>88, 89</p> <p><i>Conversion to [1-¹³C]-vitamin C illustrated in normal rat brain</i> Not yet applied to the study of brain cancer</p>

Author Manuscript

Author Manuscript

Author Manuscript

Author Manuscript

Altered Pathways	REF	HP Probe	Sequences	Use	REF
<ul style="list-style-type: none"> • 	43, 53-55	[2-¹³C, 1,2-²H₄]-choline chloride T1-60s at 3T P _{hp} -28-35%		•	101-103
<ul style="list-style-type: none"> • 	98-100	[1-4-¹³C₂]-fumarate T1-24s at 9.4T P _{hp} -26-35%		•	98-100

↓ glutathione

✓

Abnormal choline metabolism associated with IDH1 mutation

✓ ↓ PC

✓ ↑ GPC

Necrosis: increase permeability of the necrotic cell membrane

✓ ↑ uptake fumarate

✓ ↑ release fumarase enzyme

Not yet applied to the study of low-grade brain tumor

Not yet applied to the study of GBM